Appl. Phys. A
DOI 10.1007/s00339-014-8804-6

Applied Physics A
Materials Science & Processing

Ultraviolet random lasing from $Mg_{0.12}Zn_{0.88}O$:N/ZnO:Ga single-heterostructure diode

Muhammad M. Morshed · Zheng Zuo · Jian Huang · Jianlin Liu

Received: 3 July 2014 / Accepted: 23 September 2014

Abstract A heterostructure device consisting of nitrogen-doped $Mg_{0.12}Zn_{0.88}O$ and gallium-doped ZnO thin films was grown on *c*-plane sapphire substrate using RF plasma-assisted molecular beam epitaxy. Current–voltage and photocurrent characteristics indicate the formation of a p–n junction. Random lasing behavior with lasing modes centered at 356 nm was observed. A low-threshold current of 6 mA was determined, and an output power of 34 nW was measured at an injection current of 8 mA. The film contains columnar structures with much air gaps, which assist in light scattering to achieve necessary gain for random lasing.

1 Introduction

Zinc oxide (ZnO) is an excellent material for ultraviolet (UV) optoelectronics, thanks to its direct wide band gap of 3.37 eV, high exciton binding energy (60 meV) at room temperature (RT), and ease of tuning the band gap energies using compatible $Mg_xZn_{1-x}O$ and $Cd_xZn_{1-x}O$ alloys [1–5]. Recently, much effort has been invested in ZnO-based random laser research for various potential applications such as bio-sensing, speckle-free imaging, medical diagnostics, and information storage and defense [6–8]. There have been many reports of ZnO-based homojunction LED devices [9–12], and also, several ZnO-based random lasing device structures have already been demonstrated, including homojunctions, metal–insulator–semiconductor (MIS) structures, and heterostructured devices with the combination of n-ZnO and other p-type materials [13–20]. For practical applications, it is essential to significantly enhance the output power of the device and also have controllability on the wavelength of the random lasing modes [19, 21]. The central wavelength of the random lasing spectrum was tuned from ~380 to 352 nm by adjusting Mg mole fraction in $Mg_xZn_{1-x}O$ MIS structures on Si [17]. To further achieve strong light output in the UV region less than 380 nm, p–n junction type random lasers are desirable, but have not been reported.

In this study, we report random lasing of N-doped $Mg_{0.12}Zn_{0.88}O$/Ga-doped ZnO single-heterostructure p–n junction diode. N-doped $Mg_{0.12}Zn_{0.88}O$ thin film over Ga-doped ZnO layer was grown on *c*-plane sapphire substrate by RF plasma-assisted molecular beam epitaxy. Electrically pumped random lasing centered at 356 nm was observed, and an output power of 34 nW was attained at a drive current of 8 mA. The lasing mechanism is discussed.

2 Experimental details

C-plane sapphire substrate was cleaned by aqua regia (HNO_3:HCl = 1:3) solution followed by deionized water rinsing and nitrogen blow drying. The substrate was immediately introduced in an RF plasma-assisted molecular beam epitaxy system. At the beginning of growth, a MgO/ZnO bilayer of 15 nm was deposited at 450 °C as a nucleation layer. On top of this buffer, Ga-doped ZnO (400 nm) was deposited at 500 °C with Zn, Ga cell temperature, and oxygen (O_2) flow at 350, 542 °C, and 3 sccm, respectively. The plasma power was kept at 400 W. N-doped $Mg_{0.12}Zn_{0.88}O$ (250 nm) was subsequently deposited at the same substrate temperature with Zn, Mg cell temperature, and O_2/N_2O flow at 346, 435 °C, and 2.5/

M. M. Morshed · Z. Zuo · J. Huang · J. Liu (✉)
Department of Electrical and Computer Engineering, University of California, Riverside, CA 92521, USA
e-mail: jianlin@ece.ucr.edu

Published online: 01 October 2014

2.5 sccm, respectively. After the growth, the sample was in situ annealed at 600 °C for 20 min with 3 sccm of O_2 flow. Additionally, two reference thin films of $Mg_{0.12}Zn_{0.88}O$:N and ZnO:Ga were separately grown using the same growth conditions as that of the device layers. Details on the N-doped $Mg_{0.12}Zn_{0.88}O$:N thin film have been reported elsewhere [22].

Room-temperature Hall effect measurement was done for the reference samples in variable magnetic field up to 6,000 gauss. In the Hall effect measurement system, a Kiethley 6220 current source and a Kiethley 2182 voltmeter were used with minimum current capability of 0.1 pA with up to 105 V compliance and voltage capability of 1 nV, respectively. Au/Ni and Au/Ti were deposited on $Mg_{0.12}Zn_{0.88}O$:N and ZnO:Ga reference films, respectively, as contacts in Hall bar rectangular geometry, which were subsequently annealed properly using RTA process. Circular geometry mesa (450 μm diameter) structure was fabricated following the standard photolithography process. Au/Ti (150/20 nm) and Au/Ni (150/20 nm) contacts were deposited on ZnO:Ga and $Mg_{0.12}Zn_{0.88}O$:N layers, respectively, and annealed. Current–voltage (*I–V*) characteristics of the device were measured using an Agilent 4155C semiconductor parameter analyzer. Electroluminescence (EL) measurements were carried out using an EL system composing of an Oriel monochromator, a photomultiplier detector, a lock-in amplifier, and a chopper. An external HP E3630A dc power supply was used to input current for EL measurements. Photocurrent (PC) measurements were carried out using a 150-W Xe arc lamp as light source. The device was packaged on TO5 Can for EL and PC measurements. The output power of the device was measured using a Thorlabs PM100 optical power meter.

3 Results and discussion

Figure 1a shows X-ray diffraction (XRD) pattern of the $Mg_{0.12}Zn_{0.88}O$:N/ZnO:Ga sample. The peak at ~34.4° indicates that the thin film was grown preferentially along the *c*-direction of the wurtzite lattice structure, according to the standard card (JCPDS 36-1451). Figure 1b shows top-view scanning electron microscopy (SEM) image of the film. The top left inset shows cross-sectional SEM image of the film. The film exhibits closely packed columnar structures with many pits or air gaps in between these columns and an average in-plane column size of ~250 nm. The FWHM (0.2°) of the XRD peak (~34.4°) also suggests polycrystalline nature of the film [15]. This morphology originates from low quality thin MgO/ZnO buffer and subsequent low temperature growth of large lattice mismatched active layer with respect to the substrate [23].

Figure 1c shows absorption spectrum at RT of the $Mg_{0.12}Zn_{0.88}O$:N reference sample. The excitonic

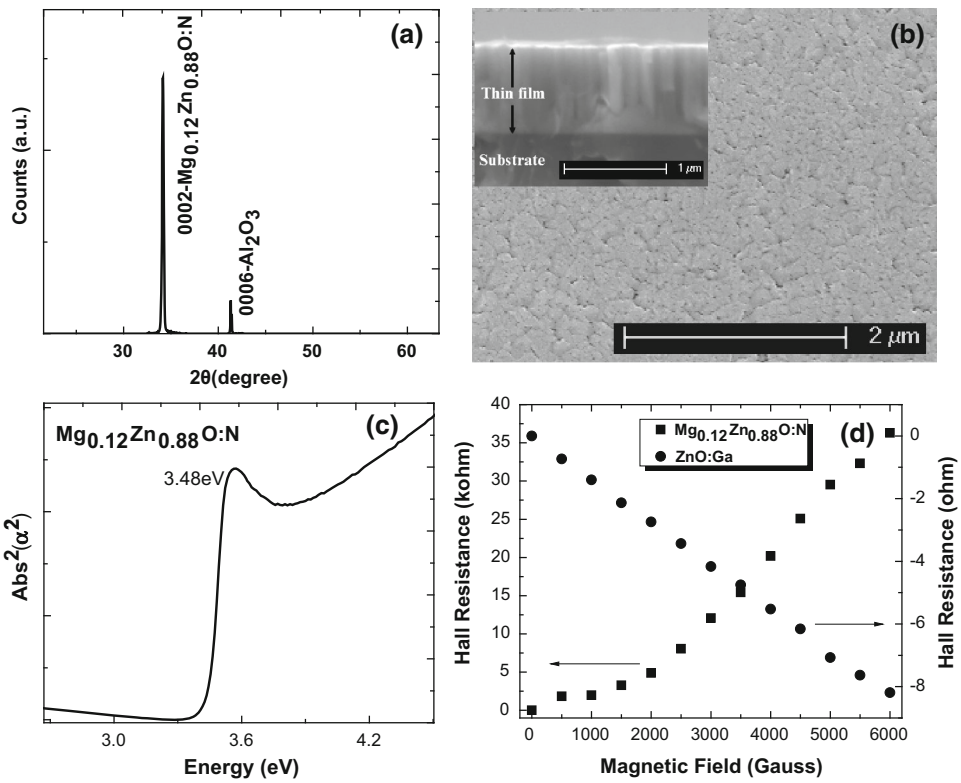

Fig. 1 **a** XRD pattern, **b** SEM image from the surface of the device. The *top left inset* shows the cross-sectional SEM image of the heterostructure. **c** Square of absorption coefficient (α) at RT of the $Mg_{0.12}Zn_{0.88}O$:N reference sample. **d** Hall resistance as a function of applied magnetic field at RT of the $Mg_{0.12}Zn_{0.88}O$:N (*left y*-axis) and ZnO:Ga (*right y*-axis) reference samples

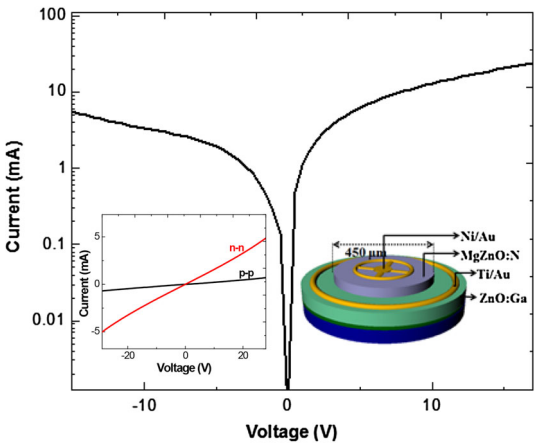

Fig. 2 *I–V* characteristics in semi logarithmic scale of the device. The *bottom left inset* shows the *I–V* curves of both n-type and p-type contacts. The *bottom right inset* shows the schematic of the device structure

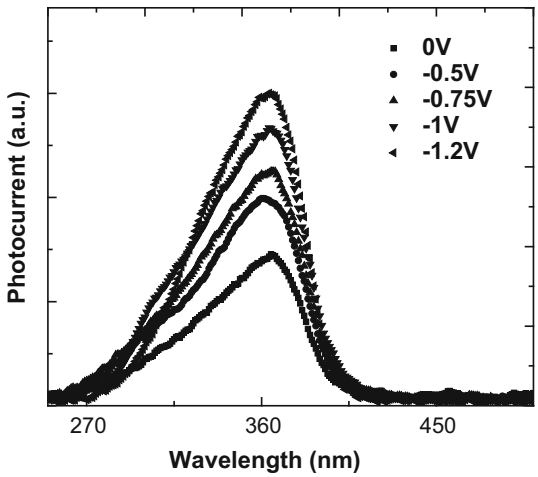

Fig. 3 Photocurrent spectra under zero and different reverse biases

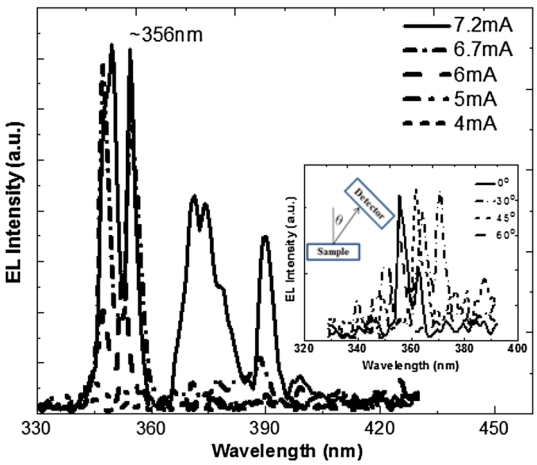

Fig. 4 Room-temperature EL spectra under different injection current. The *bottom right inset* shows angle-dependent EL spectra of the device at an injection current of 8 mA

resonance peak in the spectrum shows good optical quality, and the single slope spectrum ensures no significant phase mixing in the film. The absorption edge indicates an energy band gap of 3.48 eV. Band tailing is also visible on the lower energy side, which may be due to the presence of interband defects or nonuniform alloying effect [24, 25]

Figure 1d shows RT Hall resistance of the $Mg_{0.12}Zn_{0.88}O$:N (left *y*-axis) and ZnO:Ga (right *y*-axis) reference samples as a function of magnetic field. Positive increasing and negative decreasing Hall resistance of $Mg_{0.12}Zn_{0.88}O$:N and ZnO:Ga indicate p-type and n-type conductivity, respectively. The carrier concentration is on the order of 10^{18} cm^{-3} for ZnO:Ga and on the order of 10^{14} cm^{-3} for $Mg_{0.12}Zn_{0.88}O$:N. It should be noted that these numbers were obtained based on the electrical transport from both the active layer and buffer layer. Since the buffer layer is n-type, the true hole carrier concentration should be larger than 10^{14} cm^{-3} [22].

Figure 2 shows *I–V* characteristics of the device. The bottom left inset in Fig. 2 shows linearly dependent *I–V* curves of both n- and p-type contacts, indicating the formation of Ohmic contacts. The bottom right inset in Fig. 2 shows the schematic of the device structure. The rectifying *I–V* characteristic of the device indicates the formation of a p–n junction. Here, current starts to increase with low applied voltage showing a small threshold of around 1.5 V and rectification ratio is $\sim$10 at $\pm$ 6 V. The low threshold and rectification ratio are attributed mainly to the weak p-type behavior of the $Mg_{0.12}Zn_{0.88}O$:N layer and also partly to the trap-assisted recombination current [26, 27].

Figure 3 shows PC spectra under zero and reverse biases. The UV response extends from 270 to 390 nm. The spectra show a peak at 360 nm as most of the carriers are collected within $Mg_{0.12}Zn_{0.88}O$:N layer. A long tail response is seen on the higher energy side as the response increases proportionally to photon wavelength from 270 nm. Beyond $\sim$375 nm, corresponding to ZnO band gap at RT, the response sharply decreases as the device becomes transparent to lower energy photons. More carriers are collected with the increase of the reverse bias, leading to the increased response as shown in Fig. 3. The PC response in photovoltaic mode further supports the formation of p–n junction [28].

Figure 4 shows EL spectra with continuous dc current injection at RT. At low current injection (4–5 mA), the emission is broad and weak. With higher current injection (>6 mA), multiple emission peaks appear around 356 nm with much stronger intensity and also the line width gets narrower ($\sim$2.5 nm). The bottom right inset in Fig. 4 shows EL spectra at different detection angle under 8 mA

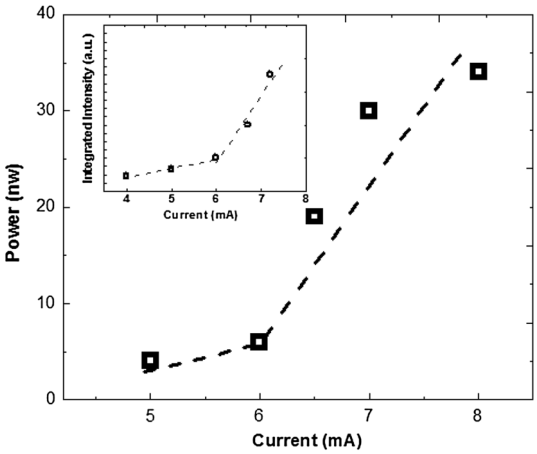

Fig. 5 Output power as a function of injection current of the device. The *left top inset* shows integrated EL intensity versus injection current. Both measurements show a threshold at around 6 mA

current injection. The spacing between adjacent peaks is different, and the peak positions also vary with different measurements. The inhomogeneous spectra indicate random nature of the emission. These amplified excitonic emissions originate from the random lasing from the device [29–31]. With higher injection current, stimulated recombination starts to occur as more holes are injected, forming more excitons. Additionally, the column boundaries with air gaps in the thin film act as the light scattering centers [16]. The emitted photons encounter multiple scattering while traveling within the thin film and achieve necessary optical gain for amplified stimulated emission. However, the limited supply of hole carriers and possible small number of close-loop gain paths may have limited the intensity and contributed to relatively broad line width of the emission.

Figure 5 shows the output power of the device as a function of injection current. The power meter was placed at the normal direction of the light emitting device. A threshold current of 6 mA is evident. The top left inset in Fig. 5 shows the integrated light intensity as a function of injection current, indicating similar threshold of around 6 mA. Light output of 34 nW was measured at a drive current of 8 mA. The measured output is limited by the fact that the detector cannot receive all the light emitted in different directions from the device.

4 Conclusion

Low-threshold random lasing was achieved from $Mg_{0.12}Zn_{0.88}O$:N/ZnO:Ga single-heterostructure device, which was grown by RF plasma-assisted molecular beam epitaxy. *I–V* and PC characteristics indicate the formation of a p–n junction. The columnar morphology of the thin film with air gaps provides the scattering media for light amplification. A threshold current of 6 mA was observed, and an output power of 34 nW was measured at a drive current of 8 mA. This work paves a way to further develop and optimize $Mg_xZn_{1-x}O$ materials and device structures for higher output power random laser operation at deeper UV wavelengths.

Acknowledgments The authors acknowledge the financial support from the Department of Energy (DE-FG02-08ER-46520).

References

1. D.M. Bagnall, Y.F. Chen, Z. Zhu, T. Yao, S. Koyama, M.Y. Shen, T. Goto, Appl. Phys. Lett. **70**, 2230 (1997)
2. S. Chu, G. Wang, W. Zhou, Y. Lin, L. Chernyak, J. Zhao, J. Kong, L. Li, J. Ren, J. Liu, Nat. Nanotechnol. **6**, 506 (2011)
3. S.F. Yu, C. Yuen, S.P. Lau, W.I. Park, G.C. Yi, Appl. Phys. Lett. **84**, 3241 (2004)
4. T. Makino, Y. Segawa, M. Kawasaki, A. Ohtomo, R. Shiroki, K. Tamura, T. Yasuda, H. Koinuma, Appl. Phys. Lett. **78**, 1237 (2001)
5. T. Takagi, H. Tanaka, S. Fujita, S. Fujita, Jpn. J. Appl. Phys. **42**, L401 (2003)
6. B. Redding, M.A. Choma, H. Cao, Nat. Photonics **6**, 355 (2012)
7. Q. Song, S. Xiao, Z. Xu, V.M. Shalaev, Y.L. Kim, Opt. Lett. **35**, 2624 (2010)
8. Q. Song, Z. Xu, S.H. Choi, X. Sun, S. Xiao, O. Akkus, Y.L. Kim, Biomed. Opt. Express **1**, 1401 (2010)
9. S. Chu, J.H. Lim, L.J. Mandalapu, Z. Yang, L. Li, J. Liu, Appl. Phys. Lett. **92**, 152103 (2008)
10. J.C. Sun, J.Z. Zhao, H.W. Liang, J.M. Bian, L.Z. Hu, H.Q. Zhang, X.P. Liang, W.F. Liu, G.T. Du, Appl. Phys. Lett. **90**, 181106 (2007)
11. S.S. Lin, J.G. Lu, Z.Z. Ye, H.P. He, X.Q. Gu, L.X. Chen, J.Y. Huang, B.H. Zhao, Solid State Commun. **148**, 25 (2008)
12. W.F. Liu, J.M. Bian, L.Z. Hu, H.W. Liang, H.Q. Zang, J.C. Sun, Z.W. Zhao, A.M. Liu, G.T. Du, Solid State Commun. **142**, 655 (2007)
13. H. Long, G. Fang, S. Li, X. Mo, H. Wang, H. Huang, Q. Jiang, J. Wang, X. Zhao, IEEE Electron Device Lett. **32**, 54 (2011)
14. J. Huang, S. Chu, J. Kong, L. Zhang, C.M. Schwarz, G. Wang, L. Chernyak, Z. Chen, J. Liu, Adv. Opt. Mater. **1**, 179 (2013)
15. S. Chu, M. Olmedo, Z. Yang, J. Kong, J. Liu, Appl. Phys. Lett. **93**, 181106 (2008)
16. J. Kong, S. Chu, Z. Zuo, J. Ren, M. Olmedo, J. Liu, Appl. Phys. A **107**, 971 (2012)
17. Y. Tian, X. Ma, P. Chen, Y. Zhang, D. Yang, Opt. Express **18**, 10668 (2010)
18. X. Ma, J. Pan, P. Chen, D. Li, H. Zhang, Y. Yang, D. Yang, Opt. Express **17**, 14426 (2009)
19. H.K. Liang, S.F. Yu, H.Y. Yang, Appl. Phys. Lett. **96**, 101116 (2010)
20. E.S.P. Leong, S.F. Yu, Adv. Mater. **18**, 1685 (2006)
21. H. Kalt, Nature Photo. **5**, 573 (2011)
22. M.M. Morshed, Z. Zuo, J. Huang, J. Zheng, Q. Lin, X. Yan, J. Liu, Appl. Phys. A (2014). doi:10.1007/s00339-014-8576-z
23. H.P. Sun, X.Q. Pan, X.L. Du, Z.X. Mei, Z.Q. Zeng, Q.K. Xue, Appl. Phys. Lett. **85**, 4385 (2004)
24. A. Janotti, C.G. Van de Walle, Phys. Rev. B **76**, 165202 (2007)
25. J. Lv, C. Li, Appl. Phys. Lett. **103**, 232114 (2013)

26. A.G. Chynoweth, R.A. Logan, D.E. Thomas, Phys. Rev. **125**, 877 (1962)
27. H.P. Maruska, D.A. Stevenson, Solid State Electron. **17**, 1171 (1974)
28. J. Huang, M.M. Morshed, Z. Zuo, J. Liu, Appl. Phys. Lett. **104**, 131107 (2014)
29. N.M. Lawandy, R.M. Balachandran, A.S.L. Gomes, E. Sauvain, Nature **368**, 436 (1994)
30. M. Kawasaki, A. Ohtomo, I. Ohkubo, H. Koinuma, Z.K. Tang, P. Yu, G.K.L. Wang, B.P. Zhang, Y. Segawa, Mater. Sci. Eng. B **56**, 239 (1998)
31. H. Cao, Waves Rand. Med. **13**, R1 (2003)